Phase-field model for front propagation in a temperature gradient: Selection and competition between the correlation and the thermal lengths

V. Popa-Nita
Faculty of Physics, University of Bucharest, P. O. Box MG-11, Bucharest 76900, Romania

P. Oswald*
Laboratoire de Physique de l'Ecole Normale Supérieure de Lyon, 46 Allée d'Italie, 69364 Lyon Cedex 07, France
(Received 30 April 2002; published 16 December 2002)

A phase-field model is presented to study the propagation and the selection of a front in directional growth. The phase transition can be first or second order and is described by a nonconserved order parameter. In general, the thermal length l_u (inversely proportional to the temperature gradient) is much larger than the correlation length l_ϕ, which gives the width of the front, and there is no direct competition between them ($\varepsilon = l_\phi / l_u \ll 1$). In this paper, we consider a situation where these two lengths can be of the same order of magnitude ($\varepsilon = l_\phi / l_u$ close to 1). This happens in liquid crystals at the nematic-cholesteric phase transition. The problem of the front selection is solved theoretically by first performing an asymptotic analysis of the governing equations in the limit $\varepsilon \to 0$, and then by solving the equations numerically. The main result is that the front is selected in a single way (no continuum of solutions) as long as $\varepsilon \neq 0$, whatever the velocity and the order of the phase transition. Finally, we show that the order parameter profile and the front temperature can change significantly when ε approaches 1.

DOI: 10.1103/PhysRevE.66.066117 PACS number(s): 05.70.Ln, 64.70.Md

I. INTRODUCTION

The phase-field formulation [1] replaces the free-boundary problem associated with the sharp interface model of an interface by a coupled pair of nonlinear reaction-diffusion equations. The spatial and temporal variations of the order parameter phase field is governed by the time-dependent Ginzburg-Landau (TDGL) equation. The second equation (for temperature) is based on a modification of the heat equation to allow a source term that accounts for latent heat production at a moving interface.

The relevant phase-field theory of liquid crystals [2,3] turns out to be just the dynamical generalization of the familiar Landau–de Gennes theory of liquid crystals interface [4]. In this paper we develop a phase-field model to study the directional solidification of a liquid crystal, in particular, a moving interphase interface as it is dragged along at a fixed, controllable velocity in a temperature gradient, which is also controllable. Even if we shall discuss the problem only from a theoretical point of view, we briefly describe the experiment [5]. A (nearly) two-dimensional sample (a thin sandwich of liquid crystal between two glass plates) is placed into a temperature gradient that points in the plane of the sample. The temperature gradient is set by putting the sample across the gap between two ovens. The temperatures of the ovens are chosen so that there is a phase transition in between, giving rise to a straight interface. The sample is set into motion at a velocity V; after a transient, the interface freezes at $-V$ in order to stay at the same temperature. We ignore the release of latent heat at the interface and assume that the temperature field is imposed by the glass plates.

All the theoretical results obtained in this paper apply to first- and second-order phase transitions described by a nonconserved order parameter ϕ. There are two typical lengths in the problem: the thermal length l_u inversely proportional to the temperature gradient and proportional to a temperature shift characteristic of the phase transition, and the correlation length l_ϕ that gives the width of the front, i.e., of the ϕ order parameter profile. In the following, we set $\varepsilon = l_\phi / l_u$. For usual phase transitions $\varepsilon \ll 1$, so that ε can be considered as the small parameter of the theory. A very classical example of first-order phase transition in liquid crystals is the nematic-isotropic phase transition. As examples of second-order phase transitions, we can cite the nematic–smectic-A transition (which can also be first order, depending on the material) and the smectic-A–smectic-C transition. In all these examples, ε is of the order of 10^{-5}. In some experiment, ε can be much larger and close to 1. This is the case at the cholesteric-nematic phase transition [6] which we describe in detail in the following section. In addition, this phase transition can be first or second order, depending on the anisotropy of the Frank elastic constants. For this reason, it constitutes an unique example of phase transition where the correlation length can be of the same order as the thermal length associated to the temperature gradient. In the following, and to present the subject in a general form, the less symmetric phase will be called as the ordered phase and the more symmetric one as the disordered phase.

This paper is organized as follows. In Sec. II, we describe the basic model and give the governing equations. In Sec. III, we study the case of a static interface in a temperature gradient when the transition is first or second order. An asymptotic analysis as a function of the small parameter ϵ is given when the phase transition is of first order. The problem is solved numerically in other cases. In Sec. IV, we discuss the case of a moving interface. This section includes an analysis of the ''pushed-pulled'' transition in free growth (at

*Author to whom correspondence should be addressed. Email address: patrick.oswald@ens-lyon.fr

zero-temperature gradient), as well as an asymptotic analysis of front selection at small ε when the transition is of first order. The equations are also solved numerically and the problem of the front selection for second-order phase transtion and first-order phase transition beyond the spinodal limit are discussed. In Sec. V, we summarize our results and present some brief conclusions.

II. THE MODEL

Within a mesoscopic approach such as ours, the free energy of a single-component system is represented by the functional

$$\mathcal{F}=\int\left[\frac{1}{2}L|\nabla\phi|^2+f(\phi,T)\right]d\vec{r}, \tag{1}$$

where L is an elastic constant, $\phi(\vec{r},t)$ the nonconserved order parameter, and T the temperature. The form of the free energy density $f(\phi,T)$ depends on the order of the phase transition [e.g., for a first-order phase transition inside the region enclosed by the spinodal, $f(\phi,T)$ has a double-well structure with respect to ϕ in which the two local minima correspond to the ordered and disordered phases].

A planar front moving in the $+x$ direction is the solution of the equations

$$\beta\,\phi_t=-\frac{\delta\mathcal{F}}{\delta\phi}=L\phi_{xx}-f_\phi, \tag{2}$$

$$T=T_0+Gx, \tag{3}$$

where β is a transport coefficient. The subscript means the differentiation with respect to that variable, G is the imposed temperature gradient, and T_0 is a reference temperature that gives the origin $x=0$ of the x axis perpendicular to the interface. $D=L/\beta$ is the diffusion coefficient of the order parameter [7].

We rewrite Eqs. (2) and (3) in the dimensionless form by scaling the free energy density: $\overline{f}=f/f_0$, where f_0 is the ''unit'' of the free energy density, and by measuring length in units of $l_\phi=(L/f_0)^{1/2}$ and time in units of l_ϕ^2/D, where l_ϕ is the width of the spatially diffuse interface region where ϕ varies rapidly. Equation (3) sets the scale of the thermal field; $l_u=\Delta T/G$, where ΔT is the characteristic temperature variation of the system. We refer to the Appendix for a precise definition of f_0 and ΔT in the two cases of first- and second-order phase transitions. Eliminating overbar, Eqs. (2) and (3) then become

$$\phi_t=\phi_{xx}-f_\phi, \tag{4}$$

$$u=u_0+\varepsilon x, \tag{5}$$

where $u=(T-T_c)/\Delta T$, $u_0=(T_0-T_c)/\Delta T$ (T_c is the phase transition temperature), and $\varepsilon=l_\phi/l_u=Gl_\phi/\Delta T$ is the (small) parameter of the theory.

In order to estimate the typical range of variation of ε in usual experiments, let us consider two typical examples. In the case of the nematic-isotropic phase transition, $\Delta T\simeq 1$ K, $G\simeq 10$ K/cm, $l_\phi\simeq 10^{-6}$ cm, so that $\varepsilon\simeq 10^{-5}$ [5,7]. The same order of magnitude is obtained for the smectic-nematic interface [8].

Much larger value of ε is expected for the cholesteric-nematic front [6]. This front is observed when a cholesteric phase is sandwiched between two parallel glass plates treated in homeotropic anchoring. This boundary condition is incompatible with the helical structure of the cholesteric phase. Because of this frustration, the helix unwinds and a homeotropic nematic phase is obtained. In usual cholesterics, the transition (of the same type as the Frederiks transition) is first order. The order parameter is the maximum tilt angle θ of the director in the sample: $\theta=0$ in the nematic and $\theta\neq 0$ in the cholesteric. The control parameter is the ratio $C=d/P$ of the sample thickness over the equilibrium cholesteric pitch. In a typical experiment, the two phases coexist at $C_c\simeq 1.1$ while the nematic phase is unstable below $C^*\simeq 0.9$. This special phase transition can be observed by changing the sample thickness (which is not convenient) or the temperature, providing that the pitch changes rapidly with the temperature. This happens near a smectic phase where the pitch diverges. In this case, it is possible to observe the transition in a sample of a given thickness and to measure the two temperatures T_c and T^* for which, respectively, the two phases coexist and the nematic phase is completely unstable. Note that in this example, the ordered phase (cholesteric) is observed at high temperature, whereas the disordered phase (nematic) occurs at low temperature (near the smectic phase). We can now estimate ε. In typical experiments, $T^*-T_c\simeq 1$ K, $l_\phi\simeq P\simeq 10^{-2}$ cm, and $G\simeq 10$ K/cm which gives $\varepsilon\simeq 0.1$. This value is much larger than with usual thermodynamic phase transitions.

In the following, we discuss comparatively the phase transition kinetics in ''free'' and ''directional'' growth. In free growth, the temperature is constant and given by T_0 or u_0 in the dimensionless form; the system responds by fixing the interface velocity. In directional growth, the sample is placed in a fixed temperature gradient and is pushed with a constant velocity. In that way, the growth velocity is imposed and the system responds by fixing the position of the interface (and hence its temperature) in the thermal gradient.

In the following, we will call v the front velocity and $u_0(v)$ the reduced temperature of the isothermal system in which the interface moves with velocity v. In directional solidification, we will take the origin of the x axis, not at T_c, but at the temperature $T_0=T_0(v)$ corresponding to the reduced temperature $u_0(v)$. This choice is more convenient from a theoretical point of view to treat the influence of the thermal gradient as a perturbation to the isothermal system. Finally, we will neglect the latent heat release and the change in temperature of the interface due to heat diffusion. It is possible to show that this assumption can always be satisfied, provided that the sample is thin enough: the front temperature is thus fixed by the glass plates limiting the sample [9].

III. STATIC INTERFACE

A. First-order phase transition

A static front only exists when the two phases have the same energy. In an isothermal system, this condition is full-

filled at the transition temperature T_c. As a consequence, we have according to our conventions $T_0=T_c$, so that $u_0=0$ and $u=\varepsilon x$ (the origin of the x axis is at T_c). By taking $f=\phi^2(1-\phi)^2+u\phi^2$, the steady form of Eqs. (4) and (5) become

$$\phi_{xx}=2\phi(1+\varepsilon x-3\phi+2\phi^2), \tag{6}$$

with the far-field boundary conditions,

$$\phi=\begin{cases}\phi_{\mathrm{ord}}=\dfrac{3}{4}\left\{1+\left[1-\dfrac{8(1+\varepsilon x)}{9}\right]^{1/2}\right\} & \text{as} \quad x\to-\infty,\\ \phi_{\mathrm{disord}}=0 & \text{as} \quad x\to\infty.\end{cases} \tag{7}$$

With this choice of f, $\phi_{\mathrm{ord}}=1$ and $\phi_{\mathrm{disord}}=0$ at T_c $(x=0)$. Note that below T_c, f has the ordered global minimum at $\phi_{\mathrm{ord}}=\frac{3}{4}\{1+(1-[8(1+u_0)/9])^{1/2}\}$. This minimum becomes metastable for $0<u_0<1/8$ and disappears for $u_0>u_0^+=1/8$ (u_0^+ is the superheating limit). The disordered fixed point $\phi_{\mathrm{disord}}=0$ is metastable for $-1<u_0<0$ and does not occur when $u_0<u_0^*=-1$ (u_0^* is the undercooling limit).

To investigate the behavior of the planar stationary interface in detail, we look for solutions of Eq. (6) for $\varepsilon\ll 1$ in the inner region corresponding to the spatially diffuse interface region where ϕ varies rapidly, and in the outer region corresponding to the bulk phases away from the interface (see Refs. [10–12] for more detailed explanation and calculation). However, a comment is in order to be done here. Because in the case of liquid crystals, the release of latent heat at the interface (and as a consequence, the change in temperature of the interface due to heat diffusion) can be neglected, the usual heat equation of the phase-field model ($u_t=D\nabla^2 u+\phi_t/2$) becomes Eq. (5) that describes the external (imposed) thermal field. The consistency of Eqs. (4) and (5) with non-negative local entropy production is no more a condition, since the system described by these equations is not isolated.

The results of the asymptotic analysis can be summarized as follows:

(i) The leading-order solution for $\tilde{\phi}_0$ in the outer region is given by

$$\tilde{\phi}_0=\begin{cases}\tilde{\phi}_{\mathrm{ord}}=\dfrac{3}{4}\left\{1+\left[1-\dfrac{8(1+\rho)}{9}\right]^{1/2}\right\} & \text{as} \quad \rho<0,\\ \tilde{\phi}_{\mathrm{disord}}=0 & \text{as} \quad \rho>0,\end{cases} \tag{8}$$

where $\rho=x\varepsilon$.

(ii) The leading order solution in the inner region is given by

$$\phi_0(x)=\frac{1}{2}\left(1-\tanh\frac{x-x_i}{w}\right), \tag{9}$$

where $w=\sqrt{2}$ is the characteristic thickness of the static interface. We mention that Eq. (9) is the solution of Eq. (6) without temperature gradient ($G=0$), but in this case the constant x_i (the location of the interface) is arbitrary.

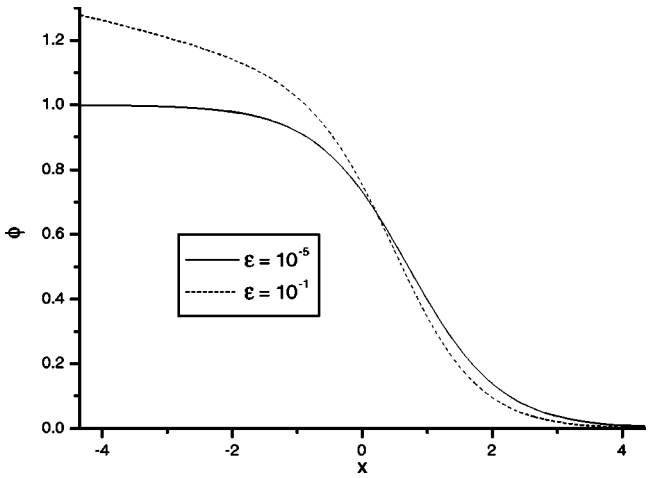

FIG. 1. The numerical profile of the order parameter for the static interface (first-order phase transition).

(iii) Solving the first-order problem in the inner region, we find the location of the interface:

$$x_i=\frac{w}{2}=\frac{\sqrt{2}}{2}. \tag{10}$$

The thermal gradient now locates the position x_i of the interface and, consequently, its temperature. Note that $\phi_0=1/2$ at $x=x_i$, where the profile has its inflexion point.

This analytical result is only valid in the limit $\varepsilon\to 0$. To obtain x_i at larger values of ε, we have solved numerically Eq. (6) using the differential equation solvers (sbval and rkfixed) of MATHCAD. Our numerical results are given in Figs. 1 and 2. Here and in the following, the numerical problem is on an infinite domain. An accurate approach would be to truncate the domain at a sufficiently large distance, rather than employing a coordinate transformation that maps the infinite interval to a finite interval. Since the significant variation of the order parameter is confined to an $O(\varepsilon)$ vicinity of the interface, we do not need to introduce a saturation term for the thermal field to determine the order param-

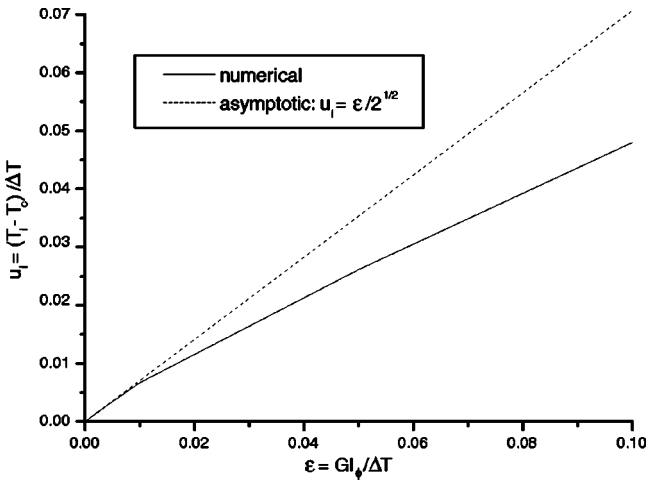

FIG. 2. The temperature of the static interface (first-order phase transition) u_i as a function of ε; comparison with asymptotic result.

eter profile. The order parameter profiles for the two limiting values of ε are shown in Fig. 1. For $\varepsilon=10^{-5}$, the numerical profile is identical with the leading-order inner region profile of the asymptotic analysis [Eqs. (9) and (10)]. For $\varepsilon=10^{-1}$, the thermal gradient influences the profile of the order parameter (especially in the wing of the ordered phase). We define the position of the interface as the value x_i of x at which the ϕ profile has an inflexion point. The reduced temperature of the interface $u_i=\varepsilon x_i$ as a function of ε is plotted in Fig. 2. The main result is that, due to the temperature gradient, the front temperature increases. For $\varepsilon \leqslant 0.005$ there is no difference between the numerical result and that given by the leading-order solution in the inner region of the asymptotic analysis [Eq. (10)]; $x_i \to \sqrt{2}/2$ and $u_i \to (\sqrt{2}/2)\varepsilon$ as $\varepsilon \to 0$. For $\varepsilon \geqslant 0.005$ the temperature increase is less important than that predicted by the asymptotic analysis at $\varepsilon \to 0$. This temperature increase of the front is small but could be experimentally observed at the cholesteric-nematic front for which $\varepsilon \simeq 0.1$.

B. Second-order phase transition

In this case, we take $f=\frac{1}{2}u\phi^2+\frac{1}{4}\phi^4$, so that the steady form of Eqs. (4) and (5) become

$$\phi_{xx}=\varepsilon x\phi+\phi^3, \tag{11}$$

with the far-field boundary conditions

$$\phi=\begin{cases}\phi_{\mathrm{ord}}=(-\varepsilon x)^{1/2} & \text{as} \quad x\to-\infty,\\ \phi_{\mathrm{disord}}=0 & \text{as} \quad x\to\infty,\end{cases} \tag{12}$$

where we have taken $u_0=0$ (the origin of the x axis is still at T_c in the temperature gradient).

In the absence of thermal gradient, the free energy $f=\frac{1}{2}u_0\phi^2+\frac{1}{4}\phi^4$ describes an ordered-disordered second-order phase transition that takes place at T_c or $u_0=0$. Below this temperature, f has the ordered global minimum at $\phi_{\mathrm{ord}}=\sqrt{-u_0}$, which disappears for $T>T_c$ (or $u_0>0$). The disordered minimum $\phi_{\mathrm{disord}}=0$ exists for $u_0>0$ and becomes a maximum when $u_0<0$. Since the two phases cannot be simultaneously stable, a well-defined interface does not exist between them, even at T_c.

On the contrary, both phases coexist in a temperature gradient with an interface in between (experimentally observed) [8,13]. To show that, we have solved numerically Eqs. (11) and (12). The numerical results are presented in Figs. 3–6. In Fig. 3 we show the numerical (continuous curve) and the far-field (dashed curve obtained by neglecting elasticity) order parameter profiles [Fig. 3(a) shows the results corresponding to $\varepsilon=10^{-5}$, while those corresponding to $\varepsilon=0.1$ are presented in Fig. 3(b)]. We use the difference between these curves to define the order-disorder interface for the second-order phase transition (plotted in Fig. 4). In Fig. 5 the width of the interface (defined as the width at half height of the difference given in Fig. 4) is plotted as a function of ε. An interesting result is that the interface width diverges in the limit $\varepsilon \to 0$. On the other hand, $w(\varepsilon)$ decreases slowly and tends to saturate at large ε. Finally, the reduced temperature u_i of the front (always defined at the inflexion point of the ϕ profile) is plotted in Fig. 6. As in the case of first-order phase transitions, the front temperature tends to increase when G increases. This effect is completely negligible with usual thermodynamic phase transitions, but could be detected experimentally at the cholesteric-nematic front, provided this transition is second order (this condition can be achieved in electric field with a liquid crystal of negative dielectric anisotropy [6]).

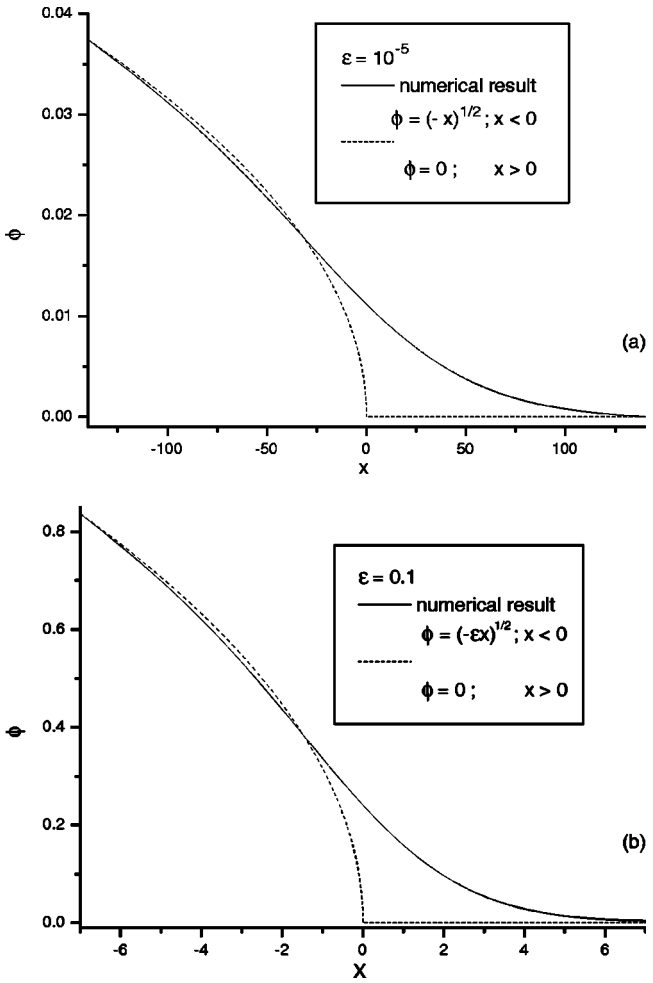

FIG. 3. The order parameter profile for the static interface (second-order phase transition); comparison with the corresponding far-field profile. The difference is used to define the interface for the second-order phase transition.

IV. MOVING INTERFACE

A. First-order phase transition

We now consider a planar ordered-disordered interface moving with a constant velocity V (in the directional solidification experiment, $-V$ is the pulling sample velocity). The dimensionless interface velocity is given by $v=Vl_\phi/D$, where l_ϕ/D is a velocity characteristic of the system (for instance, it is of the order of m/s at the solid-liquid transition in metals or plastic crystals, and of the order of mm/s at the nematic-isotropic phase transition [5,13,14]). In the frame ξ

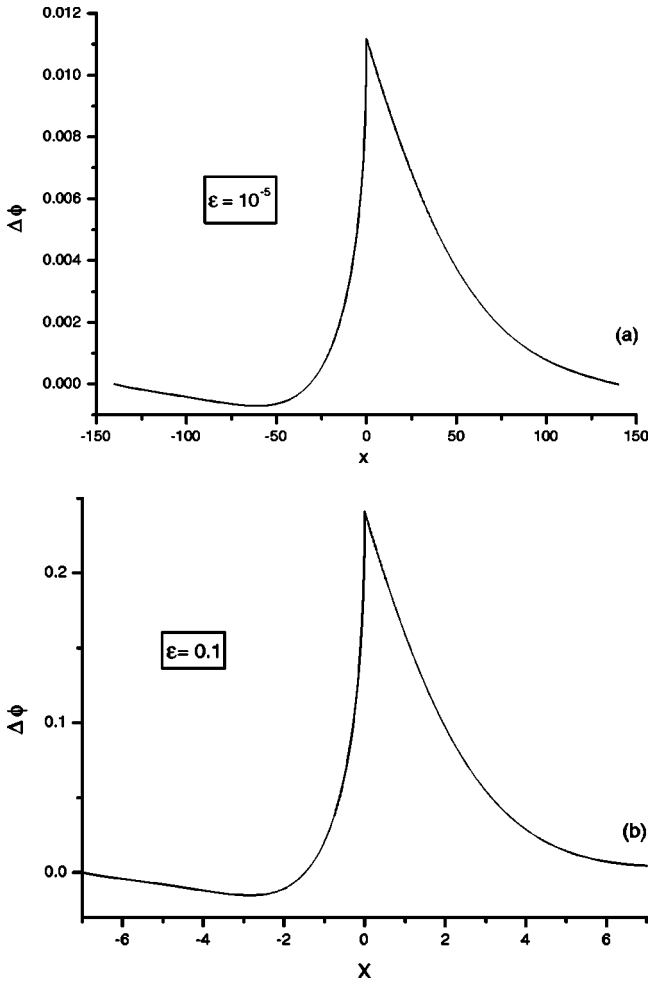

FIG. 4. The interface width for the second-order phase transition.

of the front ($\xi=x-vt$ in free growth and $\xi=x$ in directional solidification), Eqs. (4) and (5) are rewritten as

$$\phi_{\xi\xi}+v\,\phi_{\xi}=2\,\phi(1+u_0+\varepsilon\,\xi-3\,\phi+2\,\phi^2), \tag{13}$$

with the far-field boundary conditions

$$\phi=\begin{cases}\phi_{\rm ord}=\dfrac{3}{4}\left\{1+\left[1-\dfrac{8(1+u_0+\varepsilon\,\xi)}{9}\right]^{1/2}\right\} & \text{as} \quad \xi\to-\infty,\\ \phi_{\rm disord}=0 & \text{as} \quad \xi\to\infty.\end{cases} \tag{14}$$

We first recall the solution of TDGL equation (13) in the absence of a thermal gradient ($\varepsilon=0$). This solution describes the dynamics of formation of the ordered phase when the disordered phase is cooled quickly to a temperature at which it is less stable than the ordered phase. A crucial point is to know whether the system has been quenched into a region where the disordered phase is metastable ($-1<u_0<0$) or unstable ($u_0<-1$). In the temperature range $-1<u_0<0$, the stable ordered solution grows into the metastable disordered region with velocity v. The well-known solution of Eq. (13) subject to the boundary conditions

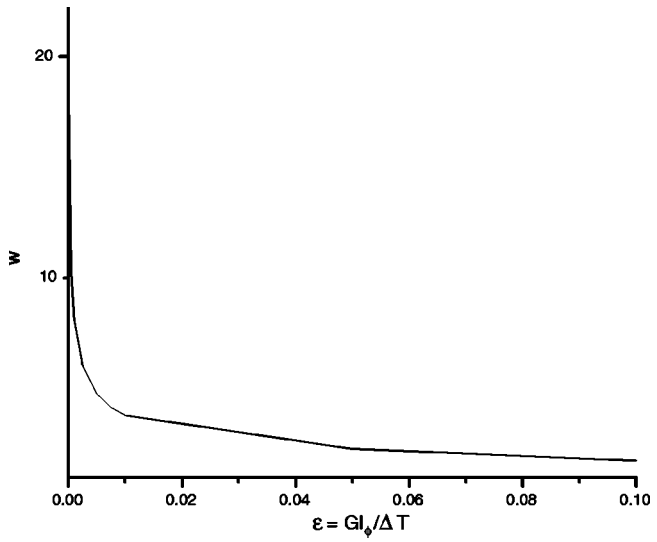

FIG. 5. The plot of the interface width for the second-order phase transition as a function of ε.

$$\phi(-\infty)=\phi_{\rm ord}=\frac{3}{4}\left\{1+\left[1-\frac{8(1+u_0)}{9}\right]^{1/2}\right\}$$

and

$$\phi(\infty)=\phi_{\rm disord}=0$$

is given by

$$\phi(\xi)=\frac{\phi_{\rm ord}}{2}\left(1-\tanh\frac{\xi-\xi_i}{w}\right), \tag{15}$$

where

$$w=\frac{\sqrt{2}}{\phi_{\rm ord}} \tag{16}$$

is the characteristic thickness of the moving interface and

$$v=3\sqrt{2}(\phi_{\rm ord}-1) \tag{17}$$

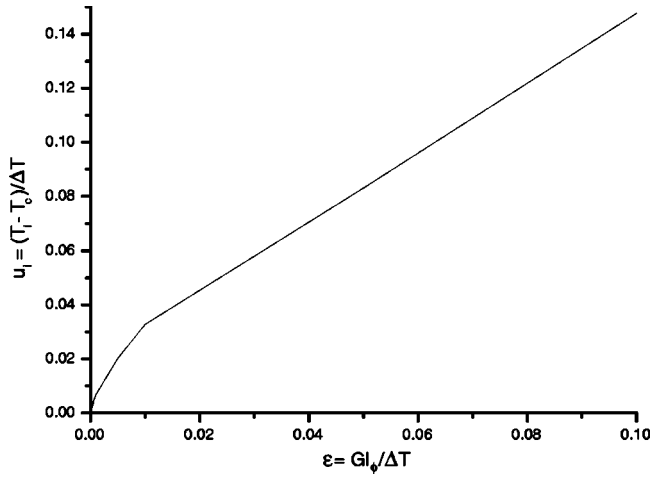

FIG. 6. The temperature of the static interface (second-order phase transition) u_i as a function of ε.

is its velocity. The constant ξ_i gives the location of the interface at time $t=0$ in the frame of the laboratory. It is arbitrary because the position of the interface is arbitrary in an isothermal system. If $u_0=0$, $\phi_{\rm ord}=1$, and $v=0$ (the two phases coexist in equilibrium, the well depths of the free energy are equal and the interface is stationary). As expected, Eq. (17) yields a positive velocity when $-1<u_0<0$ (the ordered phase grows into the disordered one) and a negative one (the ordered phase melts) when $u_0>0$. In the neighborhood of $u_0=0$, we can linearize the interface velocity in the undercooling, yielding

$$v\simeq -3\sqrt{2}u_0. \tag{18}$$

This is a well-known result of the classical Stefan model for solidification. We mention that when $-1<u_0<0$, the TDGL Eq. (13) has a discrete set of moving front solutions corresponding to lower values of velocity. The stability analysis shows that only solution (15), corresponding to the largest velocity (17), is stable and dynamically relevant [15,16].

For $u_0<-1$, the disordered phase is thermodynamically unstable. Nucleation of the order takes place through a ''phase-ordering'' kinetics process, in which the ordering takes place quickly locally, although the system retains topological defects, which it gradually expels [17]. When the disordered state is unstable, depending on the nonlinearities, one can distinguish between two regimes:

(i) Fronts whose propagation is driven (''pushed'') by the nonlinearities resemble very much to the fronts that propagate into a metastable state (''pushed'' or ''nonlinear marginal stability'' regime).

(ii) If linearities mainly cause saturation, fronts propagate with a velocity determined by linearization about the unstable state, as if they were ''pulled'' by the linear stability (''pulled'' or ''linear marginal stability'' regime) [18].

To calculate the linear marginal stability velocity, we linearize Eq. (13) around the state $\phi=\phi_{\rm disord}=0$ and write the particular solution in the form of normal modes,

$$\phi(\xi,t)=A\exp[i(k\xi-\omega t)]. \tag{19}$$

The corresponding dispersion relation reads

$$\omega=i[-2(1+u_0)-k^2], \tag{20}$$

where $u_0<-1$. When the wave number k is given real, for $0<k<\sqrt{-2(1+u_0)}$, the temporal growth rate $\omega^i(\equiv{\rm Im}\omega)$ is positive, the perturbation will grow out, and the basic front is unstable. The long-time appearance of the profile is dominated by the mode $k^r(\equiv{\rm Re}k)$ corresponding to the maximum growth rate ω^i_{max}. The condition $\partial\omega^i/\partial k^r=0$ yields $\omega^i_{max}=-2(1+u_0)+(k^i)^2$. The envelope velocity is given by $v_{\rm en}=\omega^i_{max}/k^i=-\{[2(1+u_0)]/k^i\}+k^i$ and the group velocity is $v_{\rm gr}=\partial\omega^i_{\rm max}/\partial k^i=2k^i$. If the basic front is unstable and $v_{\rm en}>v_{\rm gr}$ $[k^i<\sqrt{-2(1+u_0)}]$, at any fixed station, perturbations grow initially and, as the tail of the wave packet passed by, they ultimately decrease exponentially; the instability is convective. If the basic state is unstable and $v_{\rm en}<v_{\rm gr}$ $[k^i>\sqrt{-2(1+u_0)}]$, perturbations exponentially increase in time at any fixed station in the laboratory frame. The instability is then said to be absolute. The absolute-convective transition is reached when $v_{\rm en}=v_{\rm gr}$, the condition which yields

$$k^{i*}=\sqrt{-2(1+u_0)}\quad\text{and}\quad v^*=2\sqrt{-2(1+u_0)}. \tag{21}$$

The general properties of front propagation into unstable states drive the velocity of initially localized fronts to a selected value v^*, the so-called ''linear marginal stability velocity.'' v^* is the minimum velocity of the continuum convective instability branch (this statement can be qualitatively explained by the fact that the growth of a crystal is dominated by the growth of the slowest facet).

To describe the linear-nonlinear marginal stability (pulled-pushed) transition, we look at the asymptotic behavior of solution (15): $\phi|_{\xi\to\infty}\sim\exp(-\sqrt{2}\phi_{\rm ord}\xi)$, which yields a wave vector $k=\sqrt{2}\phi_{\rm ord}$. If $k<k^{i*}$ $(u_0<u_{0c})$, the front is moving with v^*. If $k>k^{i*}$ $(u_0>u_{0c})$, the front is moving with $v^+=3\sqrt{2}(\phi_{\rm ord}-1)$ (the nonlinear marginal stability velocity). The transition between these two regimes is reached when $k=k^{i*}$, the condition which yields the ''critical'' value of the temperature;

$$u_{0c}=-10. \tag{22}$$

For this temperature, $v^*=v^+=6\sqrt{2}$.

In directional solidification, the front is stationary in the frame of the laboratory, so that one must take $\xi=x$. The results of asymptotic analysis of Eq. (13) for $\varepsilon\ll 1$ are similar to that presented in Sec. III A for the static interface:

(i) The leading-order solution for $\tilde{\phi}_0$ in the outer region $(\rho=\varepsilon x)$ is given by

$$\tilde{\phi}_0=\begin{cases}\tilde{\phi}_{\rm ord}=\dfrac{3}{4}\left\{1+\left[1-\dfrac{8(1+u_0+\rho)}{9}\right]^{1/2}\right\} & \text{as}\quad \rho<0,\\ \tilde{\phi}_{\rm disord}=0 & \text{as}\quad \rho>0.\end{cases} \tag{23}$$

(ii) The leading-order solution for ϕ_0 in the inner region is given by

$$\phi_0(x)=\frac{\phi_{\rm ord}}{2}\left(1-\tanh\frac{x-x_i}{w}\right), \tag{24}$$

where

$$\phi_{\rm ord}=\frac{3}{4}\left\{1+\left[1-\frac{8(1+u_0)}{9}\right]^{1/2}\right\}.$$

In this expression, u_0 is the reduced temperature of the isothermal system in which the front propagates at velocity v. It is given by Eq. (17), or equivalently by

$$u_0=-\frac{\sqrt{2}}{6}v-\frac{v^2}{9}. \tag{25}$$

(iii) Solving the first-order problem in the inner region, we find the solvability condition

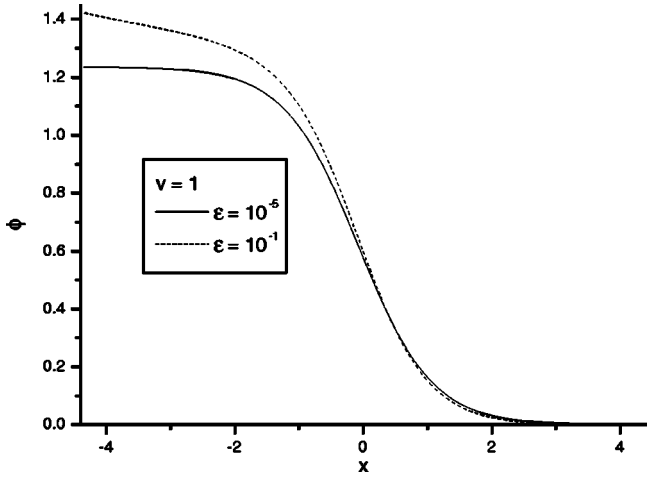

FIG. 7. The numerical profile of the order parameter (at $v=1$) for the moving interface (second-order phase transition).

$$\int_{-\infty}^{\infty} x \exp(vx)\phi_0 \frac{d\phi_0}{dx} dx = 0, \tag{26}$$

which yields $x_i(v)$ in the limit of $\varepsilon \to 0$. Note that $x_i(v)$ gives the position of the front with respect to the position $x=0$, which corresponds to the reduced temperature $u_0(v)$ given by Eq. (25). As a consequence, $x_i(v)$ [or equivalently $u_i - u_0 = (T_i - T_0)/\Delta T = \varepsilon x_i$] shows directly the effect of the thermal gradient on the front position (or on the front temperature with respect to T_0, the temperature of the isothermal system at which the front propagates at velocity v) in a directional solidification experiment.

Because this problem cannot be solved analytically, we did that numerically. The results are presented in Figs. 7–10. The order parameter profiles (at $v=1$) for the two limiting values of ε are shown in Fig. 7 (in this graph the origin of the x axis is taken at the temperature $T_0(v=1) = T_c - 0.347\Delta T$ [calculated from Eq. (25)]). The results are very similar to those obtained for a static interface in the sense that for $\varepsilon = 10^{-5}$, the numerical profile is identical with the leading-order inner profile of the asymptotic analysis [Eq. (24)], whereas the influence of the thermal gradient becomes important at $\varepsilon = 10^{-1}$. We have also plotted in Fig. 8 the reduced temperature of the interface $u_i - u_0$ as a function of

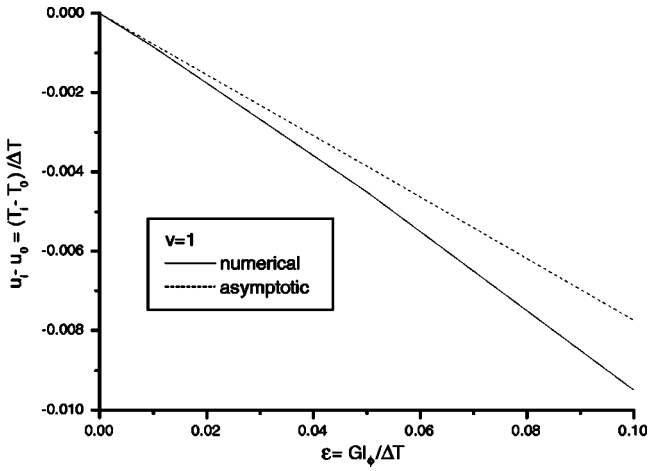

FIG. 8. The (relative) temperature of the moving interface (first-order phase transition) $u_i - u_0$ as a function of ε.

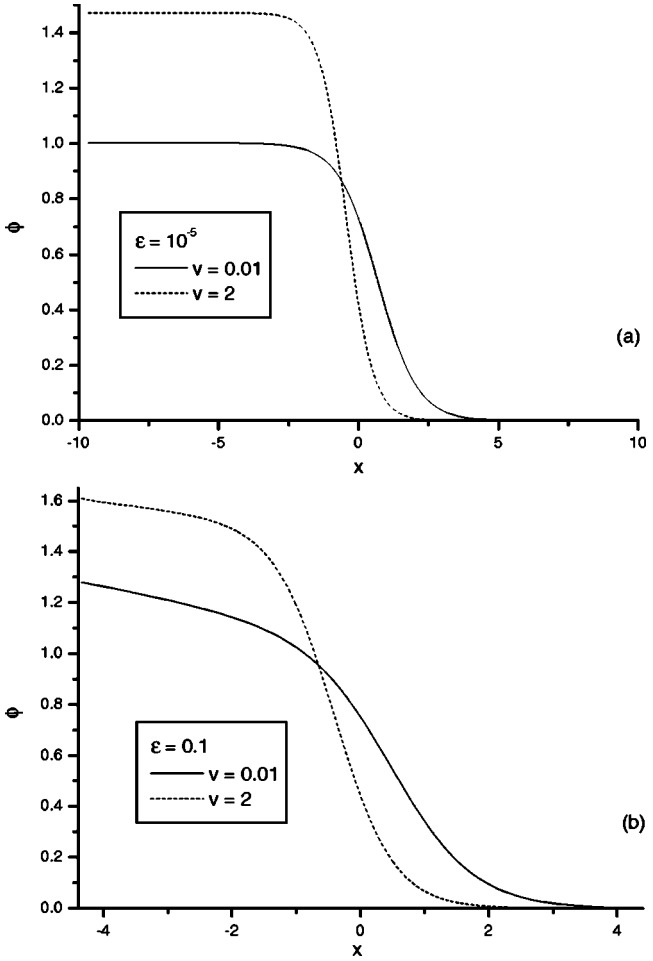

FIG. 9. Plots of the order parameter profiles (first-order phase transition) for two values of velocity.

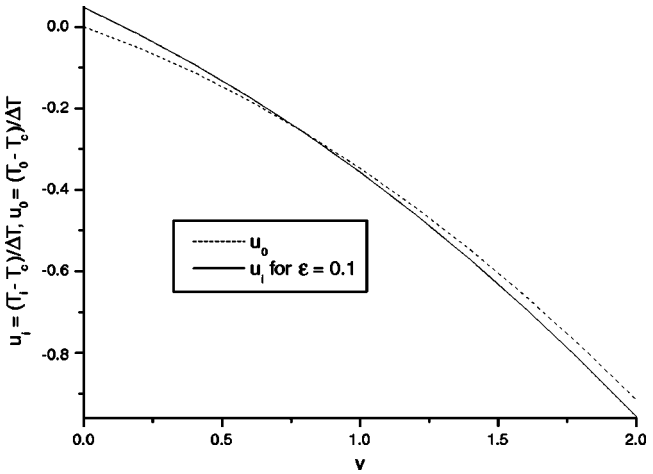

FIG. 10. Plots of the temperatures of the moving interface (first-order phase transition) in temperature gradient u_i and in an isothermal system u_0, respectively, as a function of velocity.

ε. Contrary to the static case, the thermal gradient tends to decrease the temperature of the interface at this velocity, but this effect is always very small even at large value of ε. The order parameter profiles for two values of the velocity are represented in Fig. 9 [Fig. 9(a) shows the results corresponding to $\varepsilon=10^{-5}$, while those corresponding to $\varepsilon=0.1$ are presented in Fig. 9(b)]. Again we emphasize that the origin of the x axis is not taken at the same temperature for the two curves, but at temperatures $T_0(v)$ (in reality, the two curves do not intersect if we take the same origin). The main feature of these graphs is that the interface width decreases when the velocity increases (part of this effect is also characteristic of isothermal systems [see Eq. (16)]. The influence of the thermal gradient on the interface temperature as a function of velocity is shown in Fig. 10. We mention that the curve corresponding to $\varepsilon=10^{-5}$ coincides with the u_0 curve (the influence of the thermal gradient is completely negligible in this case). The influence becomes significant (with respect to u_0) when $\varepsilon=0.1$. We distinguish two different regions: (i) at relatively small velocities ($v<0.8$), the temperature of the interface is larger than T_0, the undercooling temperature corresponding to the isothermal system, and (ii) at large velocities ($v>0.8$), the influence of the thermal gradient is in opposite direction.

B. Second-order phase transition

In directional solidification, the TDGL equation describing the second-order phase transition has the form

$$\phi_{xx}+v\,\phi_x=(u_0+\varepsilon x)\,\phi+\phi^3, \tag{27}$$

with the far-field boundary conditions

$$\phi=\begin{cases}\phi_{\mathrm{ord}}=(-u_0-\varepsilon x)^{1/2} & \text{as} \quad x\to-\infty,\\ \phi_{\mathrm{disord}}=0 & \text{as} \quad x\to\infty.\end{cases} \tag{28}$$

In the absence of thermal gradient (isothermal system), for $u_0<0$ (i.e., $T\leqslant T_c$), the TDGL Eq. (27) (in which x must be replaced by $\xi=x-vt$) describes the dynamics of formation of an ordered phase when the disordered parent phase is cooled quickly at a temperature at which the ordered phase is thermodynamically stable and the disordered phase is unstable. Due to instability of the disordered phase, the nucleation of the ordered phase takes place only through a ''phase-ordering'' kinetics process [17]. In this case, Eq. (27) has a solution for any positive value of v. From the continuous family of uniformly translating front solutions the system selects the ''pulled'' front which moves with a velocity v^* determined by the linear behavior of the dynamical equation (27) [16,18]. The origin lies in the fact that any perturbation about the unstable (disordered) phase grows out and spreads by itself. This leads to a natural spreading velocity of linear perturbations, and v^* is nothing but this velocity itself (the linear marginal stability velocity). Equation (27) gives (see the analysis presented in Sec. IV A);

$$v^*=2\sqrt{-u_0}. \tag{29}$$

The numerical results are presented in Figs. 11 and 12 for

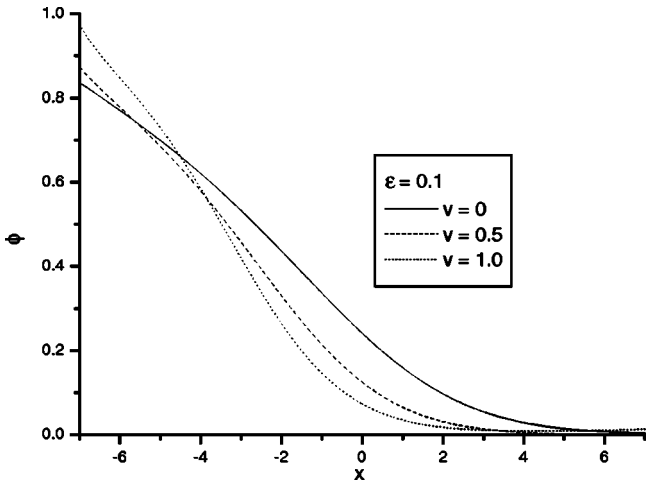

FIG. 11. The order parameter profiles (second-order phase transition) for three different values of velocity.

$\varepsilon=0.1$. In directional solidification, v is the imposed velocity. By identifying v with v^* in the corresponding isothermal system, we get from Eq. (29) the reduced temperature in this case:

$$u_0=-v^2/4. \tag{30}$$

The order parameter profiles for three different velocities are represented in Fig. 11 (with the same observation that the origin of the x axis depends on v for each profile). They show that the interface width decreases when the velocity increases. The influence of the thermal gradient on the temperature of the interface (again defined at the inflexion point of the ϕ profile) is shown in Fig. 12. Again the influence of the thermal gradient is completely negligible for $\varepsilon=10^{-5}$ (the corresponding curve coincides with the u_0 one). For $\varepsilon=0.1$, its influence becomes significant and much larger than in the case of the first-order phase transition.

Some comments are in order to be done here. For an isothermal system, the dynamics of front propagation in the

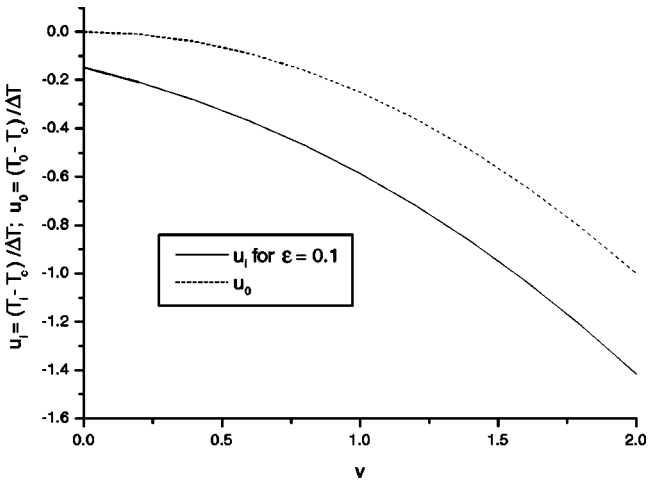

FIG. 12. Plots of the temperatures of the moving interface (second-order phase transition) in temperature gradient u_i and in an isothermal system u_0, respectively, as a function of velocity.

case of first-order phase transition [propagation of a stable (order) state into a metastable (disorder) one] is fundamentally different from that in the second-order phase transition [propagation of a stable (order) state into an unstable (disorder) one]. In the first case, the propagation of the front is driven by the nonlinearities of Eq. (13) (considered for $\varepsilon=0$), and as a consequence its velocity is ''fixed'' by the temperature. In the second case, the dynamics of the front is governed by the linearization of Eq. (27) (considered for $\varepsilon=0$) about the unstable (disorder) state, and as a consequence, there is a continous set (for any positive value of v) of solutions (the continuum convective instability branch; see Sec. IV A). To determine the front velocity, the experimental observation (that the growth of a crystal is dominated by the growth of the slowest facet) is used, and so v^* (the minimum velocity of the continuum convective instability branch, usually called the linear marginal stability velocity) is obtained.

In a thermal gradient, the velocity is imposed and the system responds by fixing the interface position x_i, and so its temperature $u_i=u_0+\varepsilon x_i$. In our calculations we have conventionally considered u_0 as the reduced temperature of the isothermal system in which the interface moves with the same velocity v [see Eq. (25) for the first-order phase transition and, respectively, Eq. (30) for the second-order phase transition]. We emphasize that the choice of u_0 is arbitrary; on the other hand, the interface temperature u_i in the thermal gradient only depends on velocity v and thermal gradient ε, and is independent of the choice of u_0. The presence of the thermal gradient does not change the main feature of the first-order phase transition concerning the propagation of the stable state into the metastable one. Thus, it may be considered as a perturbation to the isothermal system, its influence on the interface temperature being small even for large values of ε (see Fig. 10). On the contrary, the influence of the thermal gradient becomes important in the case of second-order phase transition due to the fact that now the disorder state is no longer unstable. This leads to two main differences. First, for given values of velocity v and thermal gradient ε, the system responds by selecting a well-defined front with an interface temperature u_i significantly different from the corresponding temperature u_0 of the isothermal system given by the marginal linear stability principle (see Fig. 12). Second, in the case of the second-order phase transition, for the isothermal system there is no (melting) front at temperatures larger than T_c. On the contrary, in the ''directional melting'' the front is experimentally observed and described by the model (the corresponding interface temperature as a function of velocity is shown in Fig. 13).

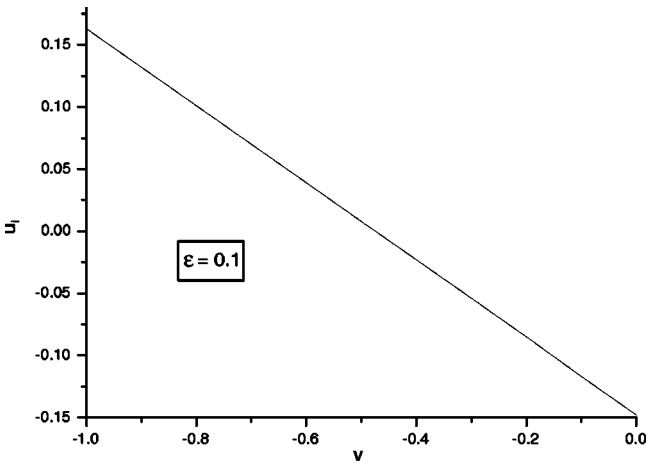

FIG. 13. The temperature u_i of the melting interface in temperature gradient as a function of velocity.

V. CONCLUSIONS

Using a Landau form of the free energy density, we have studied first- and second-order phase transitions in directional growth.

The two lengths $l_\phi=(L/f_0)^{1/2}$ and $l_u=\Delta T/G$ are characteristic of the order parameter profile and of the temperature field, respectively, and the ratio $\varepsilon=l_\phi/l_u$ is the (small) parameter of the theory.

First, we have studied the solutions corresponding to a stationary planar interface. In order to see the influence of the thermal gradient on the interface, we have studied separately the cases of first- and second-order phase transitions. In the former case, we have shown that the thermal gradient fixes the position of the interface (given by the inflexion point of the ϕ order parameter profile), which we were able to calculate analytically from an asymptotic analysis in the limit $\varepsilon\to 0$ and numerically at large ε. In the latter case (second-order phase transitions), the thermal gradient *fixes* the order parameter profile and its position. This is completely different from what happens in an isothermal system in which there is no front at T_c (at this temperature, $\phi=0$ in both phases). To define the interface width in a thermal gradient ($\varepsilon\neq 0$), we have calculated the difference between the numerical order parameter profile and the corresponding far-field profile (obtained by neglecting elasticity). The interface width diverges when $\varepsilon\to 0$ and tends to saturate at large ε.

Second, we have analyzed the moving planar interface solutions. Again, we have studied separately the two cases of first- and second-order phase transtions. In the former case, we have solved the problem of front propagation in an isothermal system: in particular, we have identified the linear-nonlinear marginal stability (pushed-pulled) transition. We have then performed an asymptotic analysis of the problem in directional growth in the limit $\varepsilon\to 0$: in this way, we have found the ϕ profile and the solvability condition that gives the position of the front in the temperature gradient. Then, we have solved numerically the problem and found that the influence of the thermal gradient becomes important when $\varepsilon\simeq 0.1$. We have observed that the interface width decreases when the velocity increases, as in isothermal systems. In the latter case of second second-order phase transitions, we have found that the front is *well selected* whatever the velocity. This result contrasts with what happens in free growth where there is a continuum of solutions at temperature lower than T_c and no front at temperature larger than T_c.

All these results need an experimental test. We think that the cholesteric-nematic front near a smectic phase is a very good candidate for doing this. Indeed, l_ϕ scales with the

cholesteric equilibrium pitch, and so can be made as large as we want by changing the concentration of chiral molecules. The order of the transition can be changed too. For instance, we can play with the anisotropy of the elastic Frank constants; although, in practice, it seems very difficult to find materials in which the transition is of second order; another method is to apply a magnetic or an electric field to a sample of negative diamagnetic or dielectric anisotropy. In this case, the field favors the chiral phase that unwinds in the nematic phase near the smectic phase because of the divergence of the twist and the bend elastic constants: it can be shown that the phase transition is second order in this case, providing that the sample is thin enough.

This model omits some features of the relevant physics. In particular, a hydrodynamical coupling between the order parameter profile and the velocity field in the medium could exist and be responsible for some unexplained instabilities observed at large velocity by Bechhoefer at the nematic-isotropic interface [19] or by Baudry at the nematic-cholesteric interface [20]. We shall address this aspect of the problem in a future work.

ACKNOWLEDGMENTS

V.P.N. is grateful for discussions with R. Holyst and D. Constantin and acknowledges support from Rhône-Alpes and CNRS grants. This work was performed while V.P.N. was visiting Ecole Normale Supérieure de Lyon, whose hospitality is gratefully acknowledged.

APPENDIX: THE LANDAU–DE GENNES FREE ENERGY DENSITIES FOR THE NEMATIC AND SMECTIC-*A* PHASES

We refer to the nematic-isotropic phase transition as an example of first-order phase transition. The corresponding Landau–de Gennes free energy density is given by

$$f=\frac{3}{2}a_N(T-T^*)\phi^2-\frac{3}{4}B_N\phi^3+\frac{9}{4}C_N\phi^4, \qquad \text{(A1)}$$

where ϕ is the scalar orientational order parameter, T^* is the undercooling limit of the isotropic phase, and the coefficients a_N, B_N, and C_N depend only on the substance (for 8CB they have the following values: $a_N=33\times10^4$ erg/K cm^3, $B_N=89\times10^5$ erg/cm^3, and $C_N=56\times10^5$ erg/cm^3 [21]).

We scale the variables in the following way:

$$\overline{\phi}=\frac{6C_N\phi}{B_N}, \quad \overline{f}=\frac{f}{\frac{B_N^4}{24^2C_N^3}}=\frac{f}{f_0},$$

$$u=\frac{24a_NC_N(T-T_c)}{B_N^2}=\frac{T-T_c}{T_c-T^*}. \qquad \text{(A2)}$$

Eliminating overbars, the nondimensional free energy density becomes

$$f=\phi^2(1-\phi)^2+u\phi^2. \qquad \text{(A3)}$$

Thus, in this case the ''unit'' of the free energy density is $f_0=B_N^4/24^2C_N^3$ and $\Delta T=T_c-T^*=B_N^2/24a_NC_N$. In 8CB, for instance, $f_0=6.2\times10^4$ erg/cm^3 and $\Delta T=1.8$ K.

On the other hand, the corresponding Landau–de Gennes free energy density for the nematic–smectic-*A* phase transition (taken here as an example of a second-order phase transition) is given by

$$f=\frac{1}{2}a_A(T-T_c)\phi^2+\frac{1}{4}C_A\phi^4, \qquad \text{(A4)}$$

where ϕ is now the smectic order parameter and T_c is the nematic–smectic-*A* phase transition temperature. For 8CB the coefficients have the following values: $a_A=5\times10^5$ erg/K cm^3 and $C_A=4\times10^6$ erg/cm^3 [21]. We scale the variables in the following way:

$$\overline{f}=\frac{f}{C_A}=\frac{f}{f_0}; \quad u=\frac{a_A(T-T_c)}{C_A}. \qquad \text{(A5)}$$

The nondimensional form of the free energy density becomes

$$f=\frac{1}{2}u\phi^2+\frac{1}{4}\phi^4. \qquad \text{(A6)}$$

In this case the ''unit'' of the free energy density is $f_0=C_A$ and $\Delta T=C_A/a_A$. In 8CB, for instance, $f_0=4\times10^6$ erg/cm^3 and $\Delta T=8$ K.

[1] For a review of phase-field models, see, e.g., A.A. Wheeler, J. Stat. Phys. **95**, 1245 (1999).
[2] V. Popa-Nita and T.J. Sluckin, J. Phys. II **6**, 873 (1996); V. Popa-Nita, T.J. Sluckin, and A.A. Wheeler, *ibid.* **7**, 1225 (1997).
[3] P. Ziherl, A. Šarlah, and S. Žumer, Phys. Rev. E **58**, 602 (1998); A. Šarlah and S. Žumer, *ibid.* **60**, 1821 (1999).
[4] P.G. de Gennes, Mol. Cryst. Liq. Cryst. **12**, 193 (1971).
[5] P. Oswald and P. Pieranski, *Les Cristaux Liquides* (Gordon and Breach Science Publishers, Paris, 2000).
[6] P. Oswald, J. Bechhoefer, A. Libchaber, and F. Lequeux, Phys. Rev. A **36**, 5832 (1987); P. Oswald, J. Baudry, and S. Pirkl, Phys. Rep. **337**, 67 (2000).
[7] P.G. de Gennes and J. Prost, *The Physics of Liquid Crystals*, 2nd ed. (Oxford University Press, New York, 1993).
[8] R. Mukhopadhyay, A. Yethiraj, and J. Bechhoefer, Phys. Rev. Lett. **83**, 4796 (1999); A. Yethiraj and J. Bechhoefer, *ibid.* **84**, 3642 (2000).
[9] J.-C. Géminard, P. Oswald, D. Temkin, and J. Malthête, Europhys. Lett. **22**, 69 (1993).
[10] G. Caginalp and X. Chen, Eur. J. Appl. Math. **9**, 417 (1998).
[11] A. Karma and W.-J. Rappel, Phys. Rev. E **53**, 3017 (1996).
[12] S.I. Hariharan and G.W. Young, SIAM (Soc. Ind. Appl. Math.) J. Appl. Math. **52**, 244 (2001).

[13] P.E. Cladis, J. Stat. Phys. **62**, 899 (1991).
[14] O.A. Gomes, R.C. Falcão, and O.N. Mesquita, Phys. Rev. Lett. **86**, 2577 (2001).
[15] J.S. Langer, Ann. Phys. (N.Y.) **41**, 108 (1967).
[16] W. van Saarloos, Phys. Rep. **301**, 9 (1998).
[17] A.J. Bray, Adv. Phys. **43**, 357 (1994).
[18] W. van Saarloos, Phys. Rev. A **37**, 211 (1988); **39**, 6367 (1989).
[19] J. Bechhoefer, Ph.D. thesis, University of Chicago, 1988 (unpublished).
[20] J. Baudry, Ph.D. thesis, Ecole Normale Supérieure de Lyon, N d'ordre 107, 1999 (unpublished).
[21] I. Lelidis and G. Durand, J. Phys. II **6**, 1359 (1996).